Table 1. 69 human cells clustered into 30 groups

Group		Title	Description	GSM
1	Normal epithelial cell,primary	NHEK-Neo1	Normal epidermal keratinocyte, neonate, primary	GSM210361
		NHBE-1	Normal bronchial epithelial cell, primary	GSM210362
2	Pulmonary epithelial cell line	A549	Pulmonary epithelial cell line	GSM210363
		BEAS-2B control (6hr)	Bronchial epithelial cell line	GSM210364
3	Lymphocyte	RPMI8226control (6hr)	B cell line	GSM210365
		Raji-1	B cell line	GSM210366
		NK92	NK cell line	GSM210367
4	Myelomonocytic leukemia	U937c	U937 control	GSM210368
		U937h	U937+HRF	GSM210369
		U937ha	U937+HRF+antibody	GSM210370
		U937a	U937+antibody	GSM210371
5	Embryonal carcinoma, cancer	NCR-G3	Embryonal carcinoma, NCR-G3, non-adherent	GSM201141
		NCR-G2NAd	Embryonal carcinoma, NCR-G2, non-adherent	GSM210373
		NCR-G4Ad	Embryonal carcinoma, NCR-G4, adherent	GSM201142
		NCR-G3Ad	Embryonal carcinoma, NCR-G3, adherent	GSM210375
6	ES cell	H1_P43	Undifferentiated hES	GSM41342
		H1-P46	Undifferentiated hES	GSM41343
		H1-P41	Undifferentiated hES	GSM41344
7	Embryonal carcinoma, cancer	NCR-G2Ad	Embryonal carcinoma, NCR-G2, adherent	GSM201140
		NCR-G1	Embryonal carcinoma, NCR-G3, non-adherent	GSM201139
8	Ewing, cancer	NCR-EW2	Ewing, cancer	GSM210378
		NCR-EW3	Ewing, ETV4, cancer	GSM210379
9	Ewing, cancer	GST6	Ewing, POU5F1, cancer	GSM201137
		GST6-extra	Ewing, POU5F1, cancer	GSM210381
10	Ewing, cancer	GST6-5az	Ewing, POU5F1, 5azaC, cancer	GSM201138
		GST6-5az-extra	Ewing, POU5F1, 5azaC, cancer	GSM210383
11	Bone marrow cell, primary	H4-1	Bone marrow cell, primary	GSM201143
		UBT5	Bmi-1, hTERT, bone marrow cell	GSM210385
		UBET7	Bmi-1, E6, hTERT, bone marrow cell	GSM210386
12	Ligament-derived cells	#10	Ligament, primary	GSM210387
	Marrow stromal cells	H10-2Vec	Vector, bone marrow cell	GSM210388
		H10-2TERT	hTERT, bone marrow cell	GSM210389
		H10-2Bmi1	Bmi-1, bone marrow cell	GSM210390
13	Placenta, primary	PL90	Placenta, primary	GSM210391
14	De-differentiated chondrocyte	TdHC1	E6, E7, hTERT, de-differentiated chondrocyte	GSM210392
15	Neural differentiated marrow stromal cell	UET13 Neural differentiation	E7, hTERT, neural differentiation, bone marrow cell	GSM210393
16	Neural differentiated marrow stromal cell	UET13 Neural differentiation1	E7, hTERT, neural differentiation, bone marrow cell	GSM210394
		UET13 Neural differentiation4	E7, hTERT, neural differentiation, bone marrow cell	GSM210395
		UET13 Neural differentiation5	E7, hTERT, neural differentiation, bone marrow cell	GSM210396
17	Cord blood-derived cells	UET13	E7, hTERT, bone marrow cell	GSM210397
		UCB408	Cord blood, primary	GSM210398
		UCB408E6E7-31	E6, E7, umbilical cord blood	GSM210399
	Adipocyte cell, primary	HAdPC1(5/21)	HAdpc1E6E7TERT28	GSM210400
18	Marrow mesenchymal cell, primary	UEET12	E6, E7, hTERT, bone marrow cell	GSM210401
		UEE16	E6, E7, bone marrow cell	GSM210402
		EPC hTERT+1	E6, E7, hTERT, endometrial cell	GSM201144
19	Cord blood, primary	UCB302	Cord blood, primary	GSM210382
		UCB302-D7	Cord blood, primary	GSM210405
		UCB302TERT	hTERT, cord blood	GSM210406
		UET9	E7, hTERT, bone marrow cell	GSM210407

Table 1. cont.

Group		Title	Description	GSM
20	Cord blood, primary	UCB408E7-32	E7, hTERT, cord blood	GSM210408
21	Fetal fibroblast, primary	HFDPC cont.	Normal follicular dermal papillar cell, primary	GSM210409
		PL112	Placenta, primary	GSM210410
		HF7-3	Fetal fibroblast, primary	GSM210411
22	Bone marrow cell, primary	3F0664	Bone marrow cell (commercial item), primary	GSM201145
		BM-MSC	Bone marrow-derived mesenchymal stem cells	GSM38627
23	ES cell-derived mesenchymal cell	H1 clone 2	ES cell-derived mesenchymal precursor	GSM38628
		H9 clone 1	ES cell-derived mesenchymal precursor	GSM38629
24	Endometrial cell	EPC100	E6, E7, hTERT, endometrial cell	GSM210413
25	Bone marrow cell, primary	Yub10F	Bone marrow cell, primary	GSM210414
26	Endometrial cell	EPC hTERT+2	E6, E7, hTERT, endometrial cell	GSM210415
		EPC Control	E6, E7, hTERT, endometrial cell	GSM210416
27	Endometrial cell	EPC214	E6, E7, hTERT, endometrial cell	GSM210417
28	Menstruation blood-derived mesenchymal cell, primary	#E4	Menstruation blood, primary	GSM210418
		#E4HRF	Menstruation blood, HRF treatment, primary	GSM210419
		#E5HRF	Menstruation blood, HRF treatment, primary	GSM210420
29	Menstruation blood-derived mesenchymal cell, primary	#E6	Menstruation blood, primary	GSM210421
		#E6HRF	Menstruation blood, HRF treatment, primary	GSM210422
30	Menstruation blood-derived mesenchymal cell, primary	#E5	Menstruation blood, primary	GSM210423

doi:10.1371/journal.pone.0002407.t001

Grem1 and DMSO were most effective at the early stage (days 1–3) of CL6 differentiation

To determine if Grem1 (125 ng/ml) functions during the early or the late stage of differentiation, CL6 cells were treated with Grem1 for different time periods (Fig. 3A). Grem1 and DMSO were most effective on CL6 differentiation at 1–3 days (Fig. 3B, C) as assessed by percentages of MF20-positive area and beating area. Since Grem1 inhibits BMPs through direct binding [24], we hypothesized that BMP signaling is inhibitory to CL6 cardiomyogenesis during days 1–3. To confirm this hypothesis, RT-PCR analysis was performed to determine expression of the early mesodermal marker (*BrachyuryT* and *Tbx6*), cardiomyocyte-specific transcription factors (*Csx/Nkx2.5*), structural genes (*β-MyHC*), and *Gapdh* (Fig. 4A). DMSO induced the *BrachyuryT* and *Tbx6* genes, and their expressions peaked at 3 days and then decreased; BMP2 down-regulated expression of these genes at 3–7 days. The *Csx/Nkx2.5* and *β-MyHC* genes started to be expressed at days 3 and 5, respectively, and their expression increased up to 14 days, at which time the timeframe analysis was terminated. BMP2 clearly inhibited expression of the *Csx/Nkx2.5* and *β-MyHC* genes (Fig. 4A, lanes 1–7 versus lanes 8–14).

To examine cardiomyogenic differentiation, immunocytochemical analysis was performed on CL6 cells treated with the inducers. CL6 cells treated with DMSO and BMP2 for the first 3 days were negative for sarcomeric myosin (MF20) at 14 days, but became positive for sarcomeric myosin, following exposure to DMSO alone during days 1–3 (Fig. 4B). To determine if DMSO induces BMP production in CL6 cells, expression levels of *Bmp2* and *Bmp4* were determined by quantitative real-time RT-PCR analysis (Fig. 4C). DMSO clearly induced the *Bmp2* and *Bmp4* genes, and DMSO-induction was inhibited by BMP2 protein. The expression level of *Bmp2* was highest during days 7–10 (Fig. 4C: *Bmp2*) in DMSO-induced CL6 cells, and that of *Bmp4* was highest during days 5–7 (Fig. 4C: *Bmp4*).

To investigate BMP signaling on cardiomyogenic differentiation, we used the *Id1* promoter-Lux plasmid that includes the luciferase gene driven by the *Id1* promoter, known as a BMP target promoter (Fig. 4D). DMSO increased BMP signaling activity that peaked at 5 days (Fig. 4D, open square). BMP2 protein increased BMP signaling activity at 3 days (Fig. 4D, closed square), but lost BMP signaling activity at 5 days and later, implying that this loss of BMP signaling leads to lack of cardiomyogenic induction.

Since Wnt/β-catenin signaling is involved in CL6 cardiomyogenesis [23,25], we hypothesized that the BMP effect on CL6 cardiomyogenesis is mediated through Wnt/β-catenin signaling. Expression of Wnt3a, an activator of canonical Wnt signaling, was indeed detected in CL6 cells exposed to DMSO, and BMP2 significantly down-regulated *Wnt3a* expression at day 3 (Fig. 4E). By using the TOPflash plasmid [23] which includes the luciferase gene driven by two sets of three copies of the TCF recognition site, Wnt/β-catenin signaling was assessed to investigate the effect of BMP2. Wnt/β-catenin signaling activity increased at 48 h after treatment with DMSO. Activity was increased by DMSO treatment but decreased by BMP2 (Fig. 4F). Time course analysis revealed that Wnt/β-catenin activity peaked at 5 days after DMSO treatment, and decreased thereafter (Fig. 4G). BMP2 inhibited DMSO-induced Wnt/β-catenin activity throughout the experimental period (up to 14 days). These results imply that BMP signaling inhibits CL6 cardiomyogenesis at the early stage through inhibition of Wnt/β-catenin signaling.

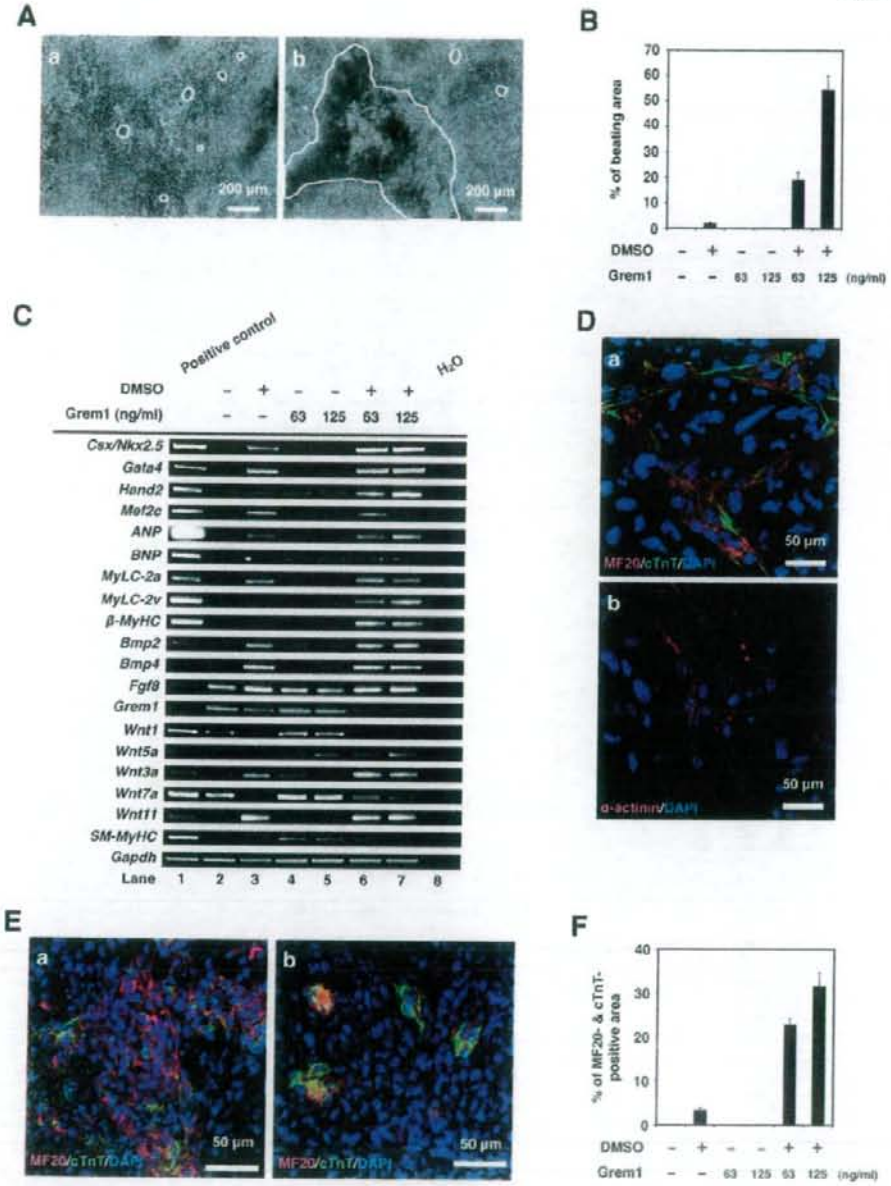

Figure 2. Grem1 enhanced cardiomyogenic differentiation in DMSO-induced CL6 cells. (A) Phase contrast micrograph of CL6 cells with exposure to DMSO alone (a), Grem1 (125 ng/ml) and DMSO (b) for 14 days. The medium, including Grem1 and DMSO, was changed every day. CL6 cells exhibited apparent spontaneous beating between days 9–11. Beating CL6 cell colonies are outlined by white lines. **(B)** Percentage of beating area in differentiated CL6 cells. CL6 cell treated with Grem1 (125 ng/ml) and DMSO exhibited the strongest contraction. **(C)** RT-PCR analysis of the genes encoding cardiac-specific transcriptional factors (*Csx/Nkx2.5, Gata4, Mef2c, Hand2*), circulating hormone (*ANP, BNP*), cardiac-specific proteins (*MyLC-2a, MyLC-2v, β-MyHC*), cytokines (*Bmp2, Bmp4, Fgf8, Grem1, Wnt1, Wnt3a, Wnt5a, Wnt7a, Wnt11*), *SM-MyHC*, and *Gapdh* (From top to bottom). Mouse total heart RNA for the *Csx/Nkx2.5, Gata4, Mef2c, Hand2, ANP, BNP, MyLC-2a, MyLC-2v, β-MyHC, Bmp2, Bmp4, Grem1, Wnt11, SM-MyHC*, and *Gapdh* genes, mouse embryonic stem cell RNA for the *Fgf8* gene, and mouse total skeletal muscle RNA for the *Wnt1, Wnt3a, Wnt5a*, and *Wnt7a* genes were used for positive controls. H_2O (without RNA) served as a negative control. **(D)** Immunocytochemistry of CL6 cells 14 days after exposure to Grem1 (125 ng/ml) and DMSO with MF20 and cTnT (a), and α-actinin (b). Cell nuclei are stained with DAPI. Clear striations are evident. **(E)** Immunocytochemistry of CL6 cells 14 days after exposure to Grem1 and DMSO with cardiac troponin T (cTnT) and sarcomeric myosin (MF20). CL6 cells treated with Grem1 (125 ng/ml) and DMSO (a), and DMSO alone (b) stained positive for cTnT and MF20. Untreated CL6 cells, i.e. not exposed to Grem1(125 ng/ml) or DMSO, stained negative for cTnT and MF20. Cell nuclei were stained with DAPI. **(F)** Percentage of MF20- and cTnT-double positive area.

doi:10.1371/journal.pone.0002407.g002

A

	Day	0	1	2	3	4	5	6	7	8	9	10	11	12	13	14
DMSO	–	–	–	–	–	–	–	–	–	–	–	–	–	–	–	–
Grem1	–	–	–	–	–	–	–	–	–	–	–	–	–	–	–	–
DMSO	1-14	–	+	+	+	+	+	+	+	+	+	+	+	+	+	+
Grem1	–	–	–	–	–	–	–	–	–	–	–	–	–	–	–	–
DMSO	1-14	–	+	+	+	+	+	+	+	+	+	+	+	+	+	+
Grem1	1-3	–	+	+	+	–	–	–	–	–	–	–	–	–	–	–
DMSO	1-14	–	+	+	+	+	+	+	+	+	+	+	+	+	+	+
Grem1	4-7	–	–	–	–	+	+	+	+	–	–	–	–	–	–	–
DMSO	1-14	–	+	+	+	+	+	+	+	+	+	+	+	+	+	+
Grem1	8-14	–	–	–	–	–	–	–	–	+	+	+	+	+	+	+
DMSO	1-3		+	+	+	–	–	–	–	–	–	–	–	–	–	–
Grem1	–	–	–	–	–	–	–	–	–	–	–	–	–	–	–	–
DMSO	1-14	–	+	+	+	+	+	+	+	+	+	+	+	+	+	+
Grem1	1-14	–	+	+	+	+	+	+	+	+	+	+	+	+	+	+
DMSO	1-14	–	+	+	+	+	+	+	+	+	+	+	+	+	+	+
Grem1	1-3	–	+	+	+	–	–	–	–	–	–	–	–	–	–	–
DMSO	1-3	–	+	+	+	–	–	–	–	–	–	–	–	–	–	–
Grem1	1-3	–	+	+	+	–	–	–	–	–	–	–	–	–	–	–

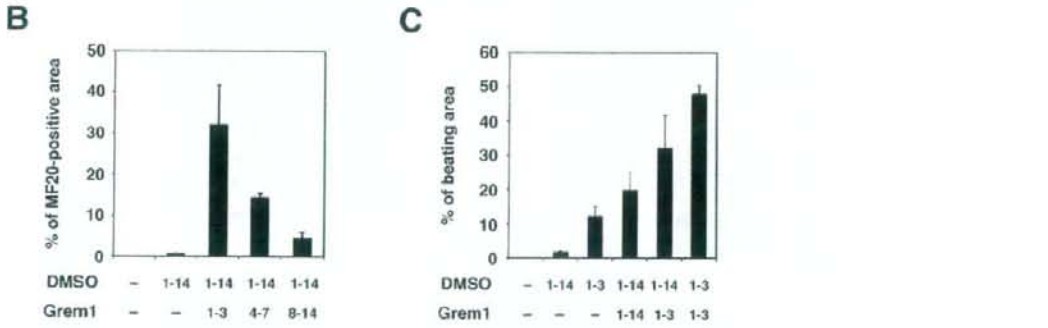

Figure 3. Percentage of myogenic differentiation by period of treatment with Grem1 in CL6 cells. (A) Protocol for treatment of Grem1 and DMSO. CL6 cells were passaged at 1.8×10^5 cells in 6-well plate on Day 0. CL6 cells were exposed to Grem1 (125 ng/ml) and/or DMSO on the indicated day. Day when the cells were exposed to the inducers is shown by "+" (in gray cells for clarity). The medium including Grem1 and DMSO was changed every day. On day 14, the cells were immunocytochemically stained with MF20 antibody. **(B)** Myogenic differentiation of CL6 cells was estimated by sarcomeric myosin (MF20)-positive area. CL6 cells were treated with Grem1 (125 ng/ml) and DMSO for the indicated days. **(C)** Myogenic differentiation of CL6 cells was estimated by beating area. CL6 cells treated with DMSO and Grem1 (125 ng/ml) were incubated at indicated days.
doi:10.1371/journal.pone.0002407.g003

Discussion

Our bioinformatics study using the results from the global gene expression analysis of human cells (GSM412342-41344 and GSM201137-201145 at http://www.ncbi.nlm.nih.gov/geo) nominated Grem1 as a candidate gene that may participate in cardiomyogenesis. By using CL6 embryonic cells as a model of cardiomyogenesis, we obtained two major findings: the first is that Grem1 enhanced cardiomyogenic differentiation of DMSO-induced CL6 cells at the early stage; the second is that Wnt/β-catenin and BMP signaling activity had developmental stage-specific effects on cardiomyogenesis (Fig. 5). Wnt/β-catenin activity at the early stage enhanced embryonic cell differentiation into cardiomyocytes, while suppressing this activity by BMP2 or BMP4 proteins as reported in the avian embryo [26]. In contrast, BMP signaling activity in the late stage enhanced cardiomyocytic differentiation. Grem1 regulated the stage-specific Wnt/β-catenin and BMP signaling activity on cardiomyogenesis.

Many studies have indicated that Grem1 is involved in cell differentiation and development, such as osteogenesis [27], lung morphogenesis [28], myogenesis [29], and limb formation [30], through inhibition of BMP2 and BMP4. Grem1-null mice show intact heart development, despite impairment of lung and kidney [31], and therefore Grem1 is considered not to be involved in cardiogenesis, or supplementary factors such as Noggin [32], with a similar function, may compensate Grem1 during development. Grem1 had an enhancing or promoting activity in *in vitro* cardiomyogenesis, as is the case with platelet-derived growth factor as a promoter of cell growth [33]. In this study, Grem1 was involved in cardiomyocyte differentiation. However Grem1 alone could not induce cardiomyocytic differentiation of CL6 cells in the absence of DMSO (Fig. 2C and F), suggesting that Grem1 is solely

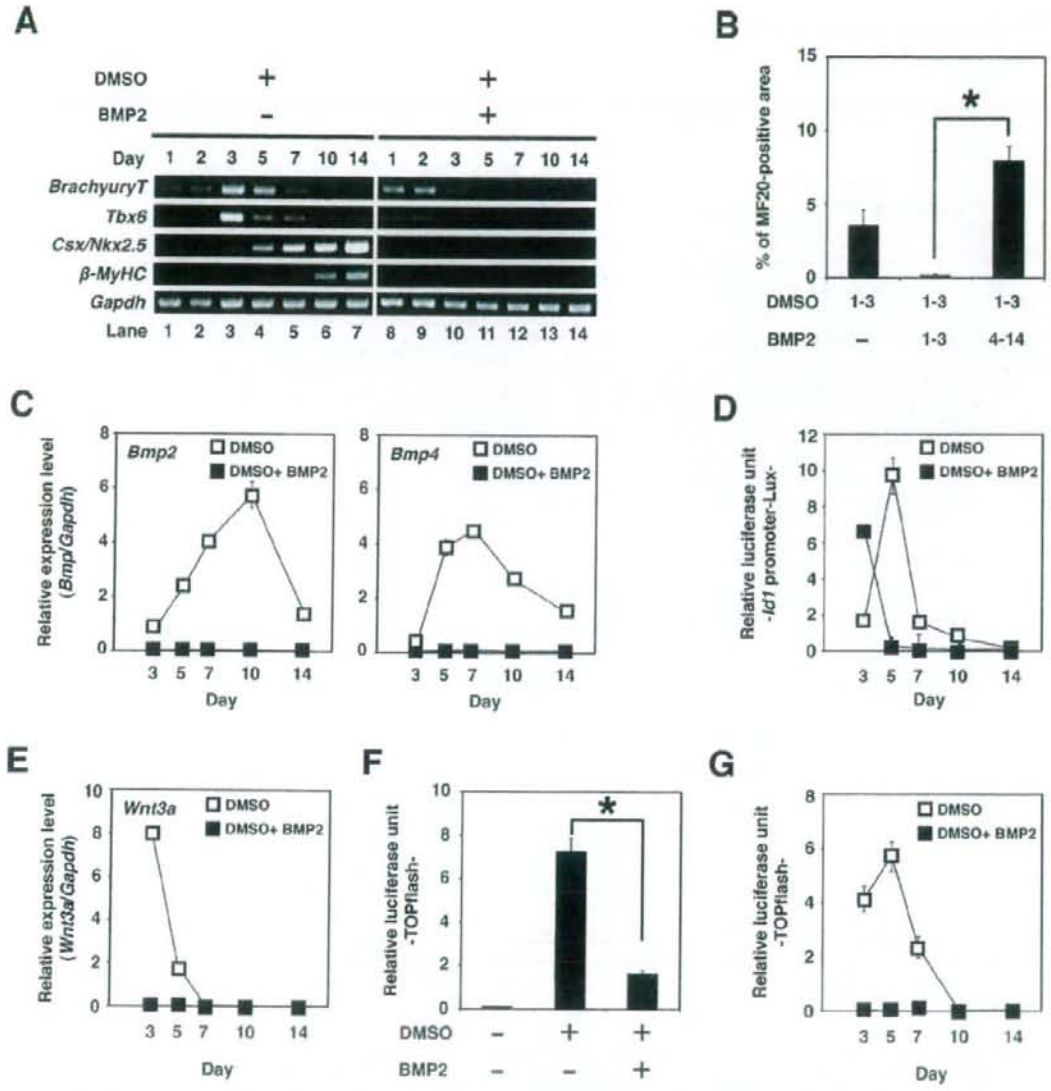

Figure 4. Cardiomyogenic differentiation in CL6 cells (days 1–3) is inhibited by BMP2. **(A)** RT-PCR analysis of the gene encoding *BrachyuryT*, *Tbx6*, cardiac-specific transcriptional factor (*Csx/Nkx2.5*), cardiac-specific protein (*β-MyHC*), and *Gapdh* (From top to bottom) of CL6 cells treated with DMSO alone, or DMSO and BMP2 (100 ng/ml) for the first 3 days (days 1–3). The medium, including BMP2 and DMSO, was changed every day. **(B)** Percentage of MF20-positive area. Immunocytochemistry was carried out on CL6 cells 14 days after cells had been exposed to DMSO and BMP2 (100 ng/ml) for the first 3 days (days 1–3). The asterisk indicates a significant statistical difference ($P<0.05$). **(C)** Quantitative real-time RT-PCR analysis of the gene encoding *Bmp2* (left), and *Bmp4* (right) in CL6 cells treated with DMSO alone (open square), or DMSO and BMP2 (100 ng/ml) (closed square) for the first 3 days (days 1–3). **(D)** BMP signaling activity of CL6 cells treated with DMSO alone (open square), or DMSO and BMP2 (100 ng/ml) (closed square) for the first 3 days (days 1–3) were determined by luciferase activity analysis using *Id1* promoter-Lux (a firefly luciferase reporter plasmid driven by the Id1 binding sites), pRL-CMV as co-transfected control, and Dual luciferase reporter assay system. Relative luciferase unit of the CL6 cells untreated with inducers at day 3 is regarded as 0.1 (data not shown). **(E)** Quantitative real-time RT-PCR analysis of the gene encoding *Wnt3a* in CL6 cells treated with DMSO alone (open square), or DMSO and BMP2 (100 ng/ml) (closed square) for the first 3 days (days 1–3). **(F)** Wnt/β-catenin signaling activity of CL6 cells 48 h after exposure to DMSO, or DMSO and BMP2 (100 ng/ml) was determined by luciferase activity analysis using TOPflash (a firefly luciferase reporter plasmid driven by two sets of three copies of the TCF binding site and herpes simple virus thymidine kinase minimal promoter), pRL-CMV as co-transfected control, and Dual luciferase reporter assay system. Relative luciferase unit of the CL6 cells untreated with inducers is regarded as 0.1. The asterisk indicates a significant statistical difference ($P<0.05$). **(G)** Timeframe of Wnt/β-catenin signaling activity in CL6 cells treated with DMSO alone (open square), or DMSO and BMP2 (100 ng/ml) (closed square) for the first 3 days (days 1–3). Relative luciferase unit of the CL6 cells untreated with inducers at day 3 is regarded as 0.1 (data not shown).

doi:10.1371/journal.pone.0002407.g004

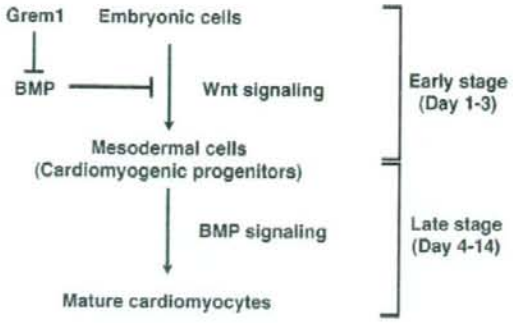

Figure 5. Grem1-accelerated CL6 cardiomyogenesis through regulation of BMP- and Wnt/β-catenin-signaling pathways. CL6 embryonic cells start to differentiate into mesodermal cells through Wnt/β-catenin signaling pathway at the early stage (days 1–3), and mesodermal CL6 cells differentiate into mature cardiomyocytes by BMP pathway at the late stage (days 4–14). Grem1 accelerates DMSO-induced cardiomyogenesis through inhibition of the BMP-signaling pathway.
doi:10.1371/journal.pone.0002407.g005

a promoter of cardiomyogenic differentiation. One of the possible mechanisms for Grem1-enhanced cardiomyogenesis at the early stage is inhibition of the BMP signaling pathway [3]. Alternatively, Grem1-enhanced cardiomyogenesis may be mediated through proliferation of cardiac progenitor cells, as is the case of myogenic progenitor proliferation by Grem1 [34], and this possibility is supported by an increased number of sarcomeric myosin-positive CL6 cardiomyocytes (Fig. 2E and F).

The stage specificity of the Grem1 effect is possibly correlated with the biphasic and antagonistic effect of Wnt/β-catenin signaling on cardiomyogenesis, depending on the stage of development *in vitro* [25] and *in vivo* [35]. CL6 cells differentiated into cardiomyocytes via mesodermal induction by the Wnt/β-catenin signaling pathway at the early stage, and CL6 mesodermal cells differentiated into cardiomyocytes induced by BMP2 at the late stage. It is conceivable that embryonic cells, such as CL6 cells and ES cells, differentiate into cardiomyocytes by inhibiting BMP signaling via putative "mesodermal cells" or "cardiomyogenic progenitors", or differentiation stages corresponding to these cells (Fig. 5, Figure S2). The early stage process from embryonic cells to mesodermal cells was mediated via Wnt/β-catenin signaling (Fig. 4F, G), and was assessed by expression of *BrachyuryT* and *Tbx6* genes (Fig. 4A), which are target genes for Wnt/β-catenin signaling [36]. BMP signaling antagonizes the cell fate-inducing activity of Wnt/β-catenin [37]. When embryonic cells or cardiomyogenic progenitors are induced to become mature cardiomyocytes by cytokines and growth factors, we must be careful with respect to the stage of cell differentiation because of the biphasic differential action of the factors which are dependent upon the differentiation stage.

In conclusion, we have demonstrated that Grem1 enhances the commitment or determined path to cardiogenic differentiation of CL6 teratocarcinoma cells. Apart from a role in development, Grem1 may serve a clinical use in cardiology, like granulocyte colony-stimulating factor that accelerates production of granulocytes in both peripheral blood and bone marrow. Nomination of *Grem1* as a cardiomyogenic factor is based on hierarchical clustering analysis using global gene expression data of human cells. This bioinformatics approach may be useful for identifying morphogens/factors that can induce differentiation of other cell types/tissues/organs.

Materials and Methods

GeneChip analysis

GeneChip analysis was performed (Fig. 1A, Table 1) as previously described [38]. Human genome-wide gene expression was examined with the Human Genome U133A Probe array (GeneChip; Affymetrix), which contains the oligonucleotide probe set for approximately 23,000 full-length genes and expressed sequence tags, according to the manufacturer's protocol (Expression Analysis technical manual and GeneChip Small Sample Target Labeling Assay version 2 technical note [http://www.affymetrix.com/support/technical/index.affx]). Data analysis was performed by the GeneChip Operation System (Affymetrix) and GeneSpringGX software (Silicon Genetics). To normalize the staining intensity variations between chips, the average difference values for all genes on a given chip were divided by the median of all measurements on that chip. Hierarchical-clustering analysis was performed using a minimum distance value of 0.001, a separation ratio of 0.5, and the standard definition of the correlation distance.

Cell culture and differentiation

CL6 cells were grown on 100 mm dishes (Becton Dickinson) in α-MEM (Gibco) supplemented with 10% fetal bovine serum (FBS) (JRH Bioscience, Inc.), penicillin, and streptomycin, and were maintained in a 5% CO_2 atmosphere at 37°C. To induce differentiation, CL6 cells were plated at a density of 1.8×10^5 cells in a 6-well plate (Becton Dickinson) or gelatin-coated 35 mm glass base dishes (IWAKI) with α-MEM containing Grem1 (63 or 125 ng/ml: R&D system) and/or 1% dimethyl sulfoxide (DMSO) for 14 days. Recombinant human bone morphogenetic protein-2 (BMP2) was purchased from R&D systems.

Reverse transcriptase-PCR (RT-PCR) and quantitative real-time RT-PCR analysis

Total RNAs were extracted from differentiated and undifferentiated CL6 cells and mouse embryonic stem (ES) cells with RNeasy minikit and DNase I treatment (QIAGEN). Mouse ES cell (129 strains) RNA, mouse heart total RNA (Clontech) and mouse skeletal muscle/total RNA (UNITECH. Co., Ltd.) were used as a positive control for each primer. Total RNA (2.0 μg each) for RT-PCR was converted to cDNA with Superscript™ III RNase H- reverse transcriptase (Invitrogen), according to the manufacturer's manual. PCR conditions were optimized and linear amplification range was determined for each primer by varying annealing temperature and cycle number. PCR products were identified by positive control size. RT-PCR was performed using the primers of the genes of cardiac specific transcription factors: *Csx/Nkx2.5*, *Gata4*, *Mef2c*, *Hand2*; circulating hormone: *ANP*, *BNP*; cardiac structural proteins: *β-MyHC*, *MyLC-2a*, *MyLC-2v*; cytokines: *Bmp2*, *Bmp4*, *Fgf8*, *Grem1*, *Wnt1*, *Wnt3a*, *Wnt5a*, *Wnt7a*, *Wnt11*; smooth muscle structural protein: smooth muscle-myosin heavy chain (*SM-MyHC*); the early mesodermal marker: *BrachyuryT*, *T-box6* (*Tbx6*); and *Gapdh* as control. PCR was performed with exTaq DNA polymerase and exTaq PCR buffer (TaKaRa) or LATaq DNA polymerase and GC buffer I (TaKaRa) for 25 or 30 cycles, with each cycle consisting of 95°C for 30 s, 50°C, 55°C, 60°C or 65°C for 45 s, and 72°C for 45 s, with an additional 5 min incubation at 72°C after completion of the final cycle. PCR primers for the genes of *Csx/Nkx2.5*, *Gata4*, *Mef2c*, *Hand2*, *ANP*, *BNP*, *β-MyHC*, *MyLC-2a*, *MyLC-2v*, *Bmp2*, *Bmp4*, *Fgf8*, *Grem1*, *Wnt1*, *Wnt3a*, *Wnt5a*, *Wnt7a*, *Wnt11*, *SM-MyHC*, *BrachyuryT*, *Tbx6*, and *Gapdh* (Table S1a) were obtained from Mouse Genome

Informatics (http://www.informatics.jax.org/). The PCR products were size-fractionated by 2% agarose gel electrophoresis.

Quantitative real-time RT-PCR was performed on an ABI Prism 7700 Sequence Detection System (Applied Biosystems), using 100 ng of cDNA in 25 μl reaction volume with 10 nmol/l of each primer, and 12.5 μl SYBR Green Realtime PCR Master Mix (TOYOBO). PCR primers for the genes of *Bmp2*, *Bmp4*, *Wnt3a*, and *Gapdh* (Table S1b) were obtained from PrimerBank (http://pga.mgh.harvard.edu/primerbank/index.html). Calculations were automatically performed by ABI software (Applied BioSystems).

Immunocytochemistry

A laser confocal microscope (LSM510, Zeiss) was used for immunocytochemical analysis. Differentiated and undifferentiated CL6 cells were fixed with 4% paraformaldehyde (Wako) for 5 min at 4°C and treated with 0.1% triton X-100 (Sigma) in PBS for 20 min at room temperature, then incubated for 20 min at room temperature in a protein-blocking solution consisting of PBS supplemented with 5% normal goat serum (DakoCytomation). These CL6 cells were then incubated overnight with primary antibody monoclonal anti-sarcomeric myosin antibody (MF20, mouse IgG_{2b}, isotype, 1 mg/ml, University of Iowa Hybridoma Bank) and Troponin T, and Cardiac Isoform Ab-1 clone 13-11 (cTnT, mouse IgG_1 isotype, 1:300, Lab Vision Corp), or the monoclonal anti-α-actinin (SARCOMERIC) CLONE EA-53 (α-actinin, mouse IgG_1 isotype, 1:300, Sigma) in PBS at 4°C. The cells were extensively washed in PBS and incubated at room temperature with Alexa Fluor 568-conjugated goat anti-Mouse IgG_{2b} (anti-MF20) (Molecular Probe; diluted 1:300), Alexa Fluor 488-conjugated goat anti-mouse IgG_1 (anti-cTnT) (Molecular Probe; diluted 1:300), Alexa Fluor 546-conjugated goat anti-mouse IgG(H+L) (anti-α-actinin) (Molecular Probe; diluted 1:300), and nuclei were counterstained with 4′, 6-diamidino-2-phenylindole (DAPI) (Wako; diluted 1:300) for 45 min. To prevent fading, cells were then mounted in DakoCytomation Fluorescent Mounting Medium (DakoCytomation).

Transfection and luciferase assays

Cells (8.0×10^5) seeded and cultured in 60 mm dishes (Becton Dickinson) were transfected 18 h after plating using Lipofectamine 2000 (Invitrogen) and PLUS reagent (Invitrogen) in Opti-MEM (Gibco). Transfection contained 1.0 μg of TOPflash plasmid (Upstate Biotechnology) for measurement of Wnt/β-catenin activity, or 5.0 μg of the *Id1* promoter-Lux plasmid (provided by Dr Imamura and Dr Miyazono) for measurement of BMP-induced *Id1* gene transcription, and 0.5 μg of pRL-CMV (Promega) as co-transfected control. Medium containing 10% FBS was changed 3 h after transfection and transfected cells (1.8×10^5) were re-seeded in 6-well plates 24 h after transfection. After 18 h, CL6 cells were induced with BMP2 (100 ng/ml) and DMSO. CL6 cells were prepared for luciferase activity analysis using Dual luciferase reporter assay system (Promega).

Area calculation

The regions of interest (beating area, immunostaining area) were defined in Photoshop (Adobe systems) using the 'magic wand' tool. The total numbers of pixels identified were then counted using the histogram function. At least five different fields were measured for each dish.

Statistical analysis

Results, shown as the mean±SE, were compared by ANOVA followed by Scheffé's test, with $P<0.05$ considered significant.

Supporting Information

Figure S1 A semi-quantitative RT-PCR of cardiomyocyte-specific genes. To investigate expression level of cardiomyocyte-specific genes (Csx/Nkx2.5, Gata4, MyLC-2a, and MyLC-2v), a semi-quantitative RT-PCR was performed from CL6 cells treated with 1% DMSO and the indicated concentration of Grem1 for 14 days. Each RT-PCR product was electrophoresed in 2% agarose gel, and was measured using ImageJ software (http://rsb.info.nih.gov/ij/) to calculate the ratio of each gene to Gapdh. The expression level for each gene is determined relative to that of Gapdh, and expression level in CL6 cells treated with DMSO alone was regarded as 1.0. The relative expression levels were averaged from at least three independent experiments.
Found at: doi:10.1371/journal.pone.0002407.s001 (1.04 MB DOC)

Figure S2 Grem1 enhanced cardiomyogenic differentiation of mouse ES cells. Mouse ES cells (NCH1.5, C57BL/6J×129ter/Sv) were cultured on a mouse embryonic fibroblast feeder layer inactivated with 30 Gy γ-irradiation in gelatin-coated 60 mm dishes (Becton, Dickinson). Cells were grown in KnockOut DMEM (Gibco) supplemented with 15% fetal bovine serum (Cell Culture Technologies), 2 mM GlutaMAX (Gibco), 0.1 mM non-essential amino acid (Gibco), 0.1 mM 2-mercaptoethanol (Gibco), penicillin, streptomycin, and 2,000 U/ml mouse leukemia inhibitory factor (LIF) (Chemicon). For cardiomyogenic differentiation, ES cells were exposed to 125 ng/ml Grem1 (R&D systems) for the three days. The cells were then trypsinized and cultured to form embryonic bodies (EBs) from a single cell using a three-dimensional culture system (without LIF) on low cell binding dishes (96-well plate round bottom). This represented day 0 of EB formation. On the next day, the medium was replaced with the same medium without LIF. EBs were re-seeded on gelatin-coated 48-well plates with one EB per well, on day 8 after the start of EB formation. The cardiomyogenic induction was estimated by the beating EB number per total EB number, measured on day 12 under a phase-contrast microscope. Grem1 increased the percentage of beating EBs to 69.2%, as compared with 26.7% in EBs without Grem1 treatment. The numbers in parentheses indicate the EB numbers counted.
Found at: doi:10.1371/journal.pone.0002407.s002 (1.27 MB DOC)

Table S1 Primer sequences.
Found at: doi:10.1371/journal.pone.0002407.s003 (0.06 MB DOC)

Movie S1 CL6 cells treated with DMSO alone. P19CL6 cells are reproducibly and stably induced into beating cardiomyocytes with DMSO.
Found at: doi:10.1371/journal.pone.0002407.s004 (1.66 MB MOV)

Movie S2 CL6 cells treated with Grem1 (125 ng/ml) and DMSO. Grem1 dramatically promotes DMSO-induced cardiomyogenic differentiation of P19CL6 cells at a concentration of 125 ng/ml.
Found at: doi:10.1371/journal.pone.0002407.s005 (2.40 MB MOV)

Acknowledgments

We would like to express our sincere thanks to T. Imamura and K. Miyazono for the *Id1* promoter-Lux plasmid, and J. Fujimoto for their discussion of this work.

Author Contributions

Conceived and designed the experiments: AU DK. Performed the experiments: DK HM RI KM. Analyzed the data: AU AN DK YT RI MT MW. Contributed reagents/materials/analysis tools: IK AN IS HS. Wrote the paper: AU DK.

References

1. Andree B, Duprez D, Vorbusch B, Arnold HH, Brand T (1998) BMP-2 induces ectopic expression of cardiac lineage markers and interferes with somite formation in chicken embryos. Mech Dev 70: 119–131.
2. Schultheiss TM, Burch JB, Lassar AB (1997) A role for bone morphogenetic proteins in the induction of cardiac myogenesis. Genes Dev 11: 451–462.
3. Angello JC, Kaestner S, Weikson RE, Buskin JN, Hauschka SD (2006) BMP induction of cardiogenesis in P19 cells requires prior cell-cell interaction(s). Dev Dyn 235: 2122–2133.
4. Alsan BH, Schultheiss TM (2002) Regulation of avian cardiogenesis by Fgf8 signaling. Development 129: 1935–1943.
5. Crossley PH, Martin GR (1995) The mouse Fgf8 gene encodes a family of polypeptides and is expressed in regions that direct outgrowth and patterning in the developing embryo. Development 121: 439–451.
6. Reifers F, Walsh EC, Leger S, Stainier DY, Brand M (2000) Induction and differentiation of the zebrafish heart requires fibroblast growth factor 8 (fgf8/acerebellar). Development 127: 225–235.
7. Whitehead GG, Makino S, Lien CL, Keating MT (2005) fgf20 is essential for initiating zebrafish fin regeneration. Science 310: 1957–1960.
8. Yamagishi H, Olson EN, Srivastava D (2000) The basic helix-loop-helix transcription factor, dHAND, is required for vascular development. J Clin Invest 105: 261–270.
9. Ariizumi T, Kinoshita M, Yokota C, Takano K, Fukuda K, et al. (2003) Amphibian in vitro heart induction: a simple and reliable model for the study of vertebrate cardiac development. Int J Dev Biol 47: 405–410.
10. Gavert N, Ben-Ze'ev A (2007) beta-Catenin signaling in biological control and cancer. J Cell Biochem 102: 820–828.
11. Chien KR, Moretti A, Laugwitz KL (2004) Development. ES cells to the rescue. Science 306: 239–240.
12. Pandur P, Lasche M, Eisenberg LM, Kuhl M (2002) Wnt-11 activation of a non-canonical Wnt signalling pathway is required for cardiogenesis. Nature 418: 636–641.
13. Yamagishi H, Yamagishi C, Nakagawa O, Harvey RP, Olson EN, et al. (2001) The combinatorial activities of Nkx2.5 and dHAND are essential for cardiac ventricle formation. Dev Biol 239: 190–203.
14. Park M, Wu X, Golden K, Axelrod JD, Bodmer R (1996) The wingless signaling pathway is directly involved in Drosophila heart development. Dev Biol 177: 104–116.
15. Marvin MJ, Di Rocco G, Gardiner A, Bush SM, Lassar AB (2001) Inhibition of Wnt activity induces heart formation from posterior mesoderm. Genes Dev 15: 316–327.
16. Schneider VA, Mercola M (2001) Wnt antagonism initiates cardiogenesis in Xenopus laevis. Genes Dev 15: 304–315.
17. Tzahor E, Lassar AB (2001) Wnt signals from the neural tube block ectopic cardiogenesis. Genes Dev 15: 255–260.
18. Olson EN (2001) Development. The path to the heart and the road not taken. Science 291: 2327–2328.
19. Terami H, Hidaka K, Katsumata T, Iio A, Morisaki T (2004) Wnt11 facilitates embryonic stem cell differentiation to Nkx2.5-positive cardiomyocytes. Biochem Biophys Res Commun 325: 968–975.
20. Sharov AA, Dudekula DB, Ko MS (2005) A web-based tool for principal component and significance analysis of microarray data. Bioinformatics 21: 2548–2549.
21. Hamatani T, Carter MG, Sharov AA, Ko MS (2004) Dynamics of global gene expression changes during mouse preimplantation development. Dev Cell 6: 117–131.
22. Sharov AA, Dudekula DB, Ko MSH (2005) http://lgsun.grc.nia.nih.gov/ANOVA/help.html#hierarchical Accessed 2007 April 20. Bioinformatics Advance Access.
23. Naito AT, Akazawa H, Takano H, Minamino T, Nagai T, et al. (2005) Phosphatidylinositol 3-kinase-Akt pathway plays a critical role in early cardiomyogenesis by regulating canonical Wnt signaling. Circ Res 97: 144–151.
24. Hsu DR, Economides AN, Wang X, Eimon PM, Harland RM (1998) The Xenopus dorsalizing factor Gremlin identifies a novel family of secreted proteins that antagonize BMP activities. Mol Cell 1: 673–683.
25. Naito AT, Shiojima I, Akazawa H, Hidaka K, Morisaki T, et al. (2006) Developmental stage-specific biphasic roles of Wnt/beta-catenin signaling in cardiomyogenesis and hematopoiesis. Proc Natl Acad Sci U S A 103: 19812–19817.
26. Jin EJ, Erickson CA, Takada S, Burrus LW (2001) Wnt and BMP signaling govern lineage segregation of melanocytes in the avian embryo. Dev Biol 233: 22–37.
27. Sutherland MK, Geoghegan JC, Yu C, Turcott E, Skonier JE, et al. (2004) Sclerostin promotes the apoptosis of human osteoblastic cells: a novel regulation of bone formation. Bone 35: 828–835.
28. Shi W, Zhao J, Anderson KD, Warburton D (2001) Gremlin negatively modulates BMP-4 induction of embryonic mouse lung branching morphogenesis. Am J Physiol Lung Cell Mol Physiol 280: L1030–1039.
29. Tzahor E, Kempf H, Mootoosamy RC, Poon AC, Abzhanov A, et al. (2003) Antagonists of Wnt and BMP signaling promote the formation of vertebrate head muscle. Genes Dev 17: 3087–3099.
30. Zuniga A, Michos O, Spitz F, Haramis AP, Panman L, et al. (2004) Mouse limb deformity mutations disrupt a global control region within the large regulatory landscape required for Gremlin expression. Genes Dev 18: 1553–1564.
31. Michos O, Panman L, Vintersten K, Beier K, Zeller R, et al. (2004) Gremlin-mediated BMP antagonism induces the epithelial-mesenchymal feedback signaling controlling metanephric kidney and limb organogenesis. Development 131: 3401–3410.
32. Yuasa S, Itabashi Y, Koshimizu U, Tanaka T, Sugimura K, et al. (2005) Transient inhibition of BMP signaling by Noggin induces cardiomyocyte differentiation of mouse embryonic stem cells. Nat Biotechnol 23: 607–611.
33. Singh JP, Chaikin MA, Pledger WJ, Scher CD, Stiles CD (1983) Persistence of the mitogenic response to platelet-derived growth factor (competence) does not reflect a long-term interaction between the growth factor and the target cell. J Cell Biol 96: 1497–1502.
34. Frank NY, Kho AT, Schatton T, Murphy GF, Molloy MJ, et al. (2006) Regulation of myogenic progenitor proliferation in human fetal skeletal muscle by BMP4 and its antagonist Gremlin. J Cell Biol 175: 99–110.
35. Klaus A, Saga Y, Taketo MM, Tzahor E, Birchmeier W (2007) Distinct roles of Wnt/beta-catenin and Bmp signaling during early cardiogenesis. Proc Natl Acad Sci U S A 104: 18531–18536.
36. Yamaguchi TP, Takada S, Yoshikawa Y, Wu N, McMahon AP (1999) T (Brachyury) is a direct target of Wnt3a during paraxial mesoderm specification. Genes Dev 13: 3185–3190.
37. Kleber M, Lee HY, Wurdak H, Buchstaller J, Riccomagno MM, et al. (2005) Neural crest stem cell maintenance by combinatorial Wnt and BMP signaling. J Cell Biol 169: 309–320.
38. Sugiki T, Uyama T, Toyoda M, Morioka H, Kunz S, et al. (2007) Hyaline cartilage formation and enchondral ossification modeled with KUM5 and OP9 chondroblasts. J Cell Biochem 100: 1240–1254.

Ultrasound Gene Transfer into Fibroblast Cells under Microbubble

Yoji Nakamura (University of Tokyo, Japan)

Ultrasound is applied to a medical field. It has the strong advantage of noninvasiveness and high-selectivity. The gene transfer using the ultrasound is one of its applications. The ultrasound has a potential to deliver some therapeutic materials, such as genes, drugs or proteins into cells. And it is known that microbubbles can improve the delivery efficiency. It is considered that the therapeutic materials can pass through the cell membrane whose permeability is increased by the destruction or oscillation of microbubbles. In this study, we tried to deliver the GFP plasmid into the fibroblast cells. Cells were cultured in six-well culture plates and exposed to the ultrasound (frequency = 2.1-MHz, wave pattern = duty cycle 10 %, intensity = 0-26 W/cm^2, time = 0-200 sec) transmitted through the medium, which contained microbubbles (Levovist® (void fraction : 8x10-4) or Sonazoid® (void fraction : L. And weμg/μ0-24x10-5) and GFP plasmid at a concentration of 15 measured the number density of microbubbles after the ultrasound irradiation. When the ultrasound intensity was increased with Levovist® 8x10-4, the transfection efficiency raised, the cell viability went down and the microbubbles disappeared. In case of Sonazoid®, the efficiency and the cell viability was nearly flat and the microbubble didn't disappeared but decreased. With the raise of the ultrasound irradiation time or microbubble density, the efficiency also raised . It is considered that microbubble destruction had a main effect to the gene transfection under Levovist® and microbubble oscillation had a main effect under Sonazoid®.

可視化情報 Vol. 28 Suppl. No. 2 (２００８年10月)

C701

超音波遺伝子導入の蛍光顕微鏡による可視化

橘 理恵*(東大), 岡本 旭生, 霞仲 潔, 高木 周, 松本 洋一郎

Visualization of Sonoporation with a fluorescence microscope

Rie TACHIBANA (Univ. Tokyo), Akio OKAMOTO, Kiyoshi YOSHINAKA,
Shu TAKAGI, Yoichiro MATSUMOTO

ABSTRACT

Recently, the development of an ultrasound gene transfer system, called Sonoporation has been investigated. It is known that micro-bubble can enhance gene transfection. Using this method, we are able to reduce cell damage, and induct genes into only target cells. However, the mechanism and optimal induction condition have not been clarified in detail. In vitro, we inducted GFP-plasmid into fibro-blast cell (NIH3T3) by using ultrasound contrast agent (micro-bubble) and piezoelectric transducer. We examined what factors affect gene induction rate. Average induction rate in whole a cell culture plate was measured with flow cytometer. Though, because of heterolytic sound pressure in a cell culture plate, measurement of partial gene induction rate is needed in order to examine the effect of sound pressure on induction rate more accurately. We stained cell nucleus and tried to measure the partial induction rate from fluorescence observation.

Keywords : Micro-bubble, Sonoporation, Fluorescence observation

1. 序論

近年，遺伝子治療において，低侵襲で目的の部位のみの細胞に遺伝子を導入することができる超音波を用いた手法が期待されている．この手法おいて，超音波造影剤として臨床的に用いられているマイクロバブルを併用することで導入効率を飛躍的に改善できるという知見が得られている．

このマイクロバブルを援用した超音波遺伝子導入のメカニズムとしては，超音波照射によりマイクロバブルが崩壊し，崩壊に伴って発生する局所的な高圧力により，細胞表面に小さな穴が空き，この小孔を通って物質輸送が行われると言われている[1]．また，超音波の圧力振動やマイクロバブルの振動により細胞膜の物質透過率が上昇することで遺伝子や粒子などが細胞内に導入される[2]とも言われているが，詳細な導入メカニズムは明らかにされていない．

本研究では，超音波とマイクロバブルによる細胞への遺伝子導入メカニズムを解明するために，超音波照射条件を変えて遺伝子導入を行うことで，いかなる因子が導入効率を高めるのかを調べることを目的とする．

2. 実験および実験装置

2.1 細胞

本研究では，遺伝子の導入細胞として線維芽細胞(NIH3T3)を用いた．線維芽細胞は多機能な未分化細胞で，軟骨への分化誘導遺伝子を細胞外から導入することで軟骨組織の再生治療へ応用が期待されている．

2.2 遺伝子

導入遺伝子は，クラゲの発光タンパク発現に関わる遺伝子から抽出され円環上の遺伝子に作りかえられた GFP プラスミドを用いた．GFP プラスミドは，細胞内に導入されると発光タンパクを発現し緑色に蛍光する．

2.3 マイクロバブル

マイクロバブルとして超音波造影剤である Sonazoid® を用いた．内部気体が C_4F_{10} で，シェル成分が脂質の気泡である．気泡径は 2.3 ～2.9 μm である．

2.4 実験装置

Fig.1 に実験装置の概略図を示す．細胞は 24well プレート内で培養した．ファンクションジェネレータ(NF 社製 WF1944A)からのバースト波をアンプ(E&I 社製 2100L)により，出力を増幅させて，トランデューサから平面波として，超音波を発生させた．周波数は 2.00 MHz とし，Duty Cycle 10 %(40/360)のバースト波として照射した．マイクロバブルと GFP プラスミド(15 μg/mL)を混合した培

発溶液にトランスデューサを浸し，上から超音波を照射した．

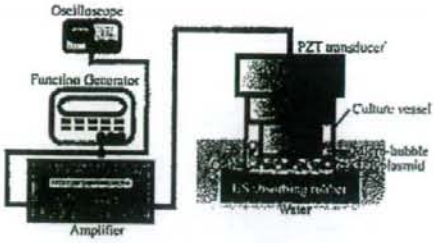

Fig.1 Experimental apparatus

3. 結果

3.1 フローサイトメトリによる導入率測定

超音波強度による導入率変化をフローサイトメータ(BD 社製 LSRⅡ)により測定した．結果を Fig.2 に示す．音圧測定により求めた培養容器全体の平均の超音波強度とファンクションジェネレータの出力との対応関係を Fig.3 に示す．これから超音波強度を大きくなるほど導入率が増加するということが分かる．しかしながら，超音波照射時に死亡してしまった細胞は培養容器の底からはがれてしまい，測定時に回収されないため，ここでの導入率はあくまで生き残った細胞のうちの遺伝子導入率である．

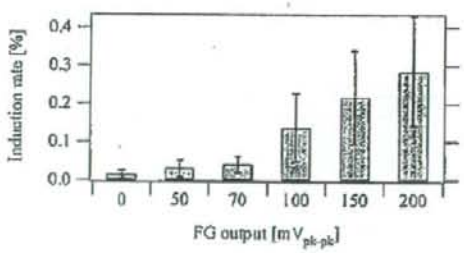

Fig.2 The effect of US intensity on induction rate
(US exposure time 60 [s], CA density 10[%])

FG output [mV$_{pk-pk}$]	0	50	70	100	150	200
US average intensity [W/cm^2]	0.00	0.44	0.86	1.76	3.97	7.06

Fig.3 US average intensity

3.2 蛍光観察による導入率測定

音圧測定により細胞容器内では圧力分布が一様ではないことが分かっている．しかしながら，フローサイトメトリによる導入率測定では容器内全体での平均導入率を測定しているため，導入率と超音波による音圧との正確な対応付けがなされていない．遺伝子導入された細胞数は GFP によりカウントできる(Fig.4(a))ので，容器内での部分的導入率測定のため，核染色(Hoechst33342)により細胞数をカウントし(Fig.4(b))，導入率測定可能にした．

蛍光観察により遺伝子導入された細胞が局所的に固まって導入されていることが多く，部分的には平均導入率の 10 倍以上の導入がなされていることが分かった．これは GFP プラスミドが培養液に均一に混ざっていないための可能性もある．今後，well 全体を蛍光画像にて撮影し，音圧分布と導入率の相関を調べること，GFP プラスミド濃度の導入率に対する影響を調べることを課題とする．

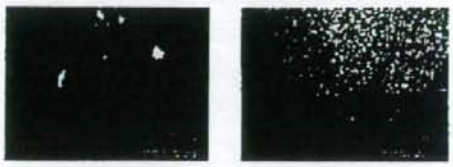

(a) induced cell (GFP) (b) cell nucleus

Fig.4 Fluorescent observation
(FG output 100 [mV$_{pk-pk}$], US exposure time 60 [s], CA density 10 [%])

4. 結言

超音波強度が大きいほど，超音波照射下において生き残った細胞中への導入率が大きくなることが示された．また，蛍光観察により，well 全体では 0.1 ～ 0.3 %の導入率であっても，局所的には数 %以上の導入率を示す可能性があることが分かった．

謝辞

本研究の一部は，文部科学省「ナノバイオインテグレーション(CNBI)」，ならびに科学研究費補助基盤研究(A)1820620 による支援を受けました．ここに謝意を表します．

参考文献

1) Taniyama et. al, "Local Delivery of Plasmid DNA Into Rat Carotid Artery Using Ultrasound", Circulation. 2002, pp.1233-1239.

2)田渕圭章, "超音波誘導遺伝子治療", 超音波テクノ, pp.203-208

2　マイクロバブルを援用した超音波遺伝子導入に関する研究

橘　理恵　　東京大学大学院

近年，遺伝子治療にむけ，低侵襲で目的の部位のみの細胞に遺伝子を導入することができる超音波を用いた手法が期待されている．この手法おいて，超音波造影剤として臨床的に用いられているマイクロバブルを併用することで導入効率を飛躍的に改善できるという知見が得られている．しかしながら，この導入のメカニズムは明らかにされていない．本研究ではマウス線維芽細胞に GFP プラスミドを，超音波照射時の条件を変化させて導入することで，いかなる因子が導入効率を高めるのかを調べた．結果は，超音波強度が大きいほど，また照射時間が長いほど，超音波照射下において生き残った細胞中への導入率が大きくなることが示された．さらに，蛍光観察により，well 全体では 0.1 ～ 0.3 %の導入率であっても，局所的には数 %以上の導入率を示す可能性があることが分かった．

キャビテーションに関するシンポジウム(第 14 回)
2009.3.19-20・仙台市

マイクロバブルを援用した超音波遺伝子導入に関する研究

A Study of Micro-bubble Enhanced Sonoporation

○橘　理恵（東京大学工学系研究科），岡本　旭生，鐘仲 潔，高木　周，松本　洋一郎
Rie TACHIBANA, The University of Tokyo, Department of Mechanical Engineering, 7-3-1 Hongo Bunkyo-ku, Tokyo 113-8656
Akio OKAMOTO, Kiyosi YOSHINAKA, Sho TAKAGI, Yochiro MATSUMOTO

Recently, the development of an ultrasound gene transfer system, called Sonoporation has been investigated. It is known that micro-bubbles can enhance gene transfection. It is thought that gene is inducted into cells by cavitation-bubble or micro-bubble collapse. However, the mechanism and optimal induction condition have not been clarified in detail. In vitro, we inducted GFP-plasmid into fibro-blast cell (NIH3T3) by using ultrasound contrast agent (micro-bubble) and piezoelectric transducer. We examined what factors affect gene induction rate. The stronger or longer ultrasound exposure is, the higher gene induction ratio is. However, the ratio is less than 1 %. It is showed that about 80 % cells are alive and that many cells get holes. Therefore, it is suggested that less genes enter into cells or genes hardly expressed.

Key Words: Cavitation, Micro-bubble, Sonoporation, Ultrasound

1. 緒言

近年，医療・生化学・生物学等の進歩により，多くの疾患の原因が遺伝子異常に由来すると明らかになってきている．これらの疾患の治療法の一つとして遺伝子治療が注目されている．遺伝子治療では細胞への遺伝子導入をいかに行うかが課題となる．現在さまざまな遺伝子導入手法が確立されているが，副作用の危険性や侵襲性といった問題点を抱えている．そこで近年注目されているのが超音波を用いた遺伝子導入法である．この手法を用いることで低侵襲な遺伝子導入が可能となる上，導入部位の選択も可能となる．

超音波遺伝子導入法はマイクロバブルを併用することで導入効率が向上することが知られている．この原理はキャビテーションバブルやマイクロバブルの崩壊時に細胞膜表面に向かって気泡内に液柱ジェットが生じ，その圧力によって細胞膜に小孔が形成され，遺伝子が導入されると考えられているが[1]，詳細な機序は不明である．

本研究の最終目標はマイクロバブルを援用した超音波遺伝子導入の機序の解明，及び，より低侵襲・高効率な手法の開発である．そのためにはまず，超音波照射時の条件変化による遺伝子導入率変化の確認を行うとともに，遺伝子導入現象を分析的に検討することで導入率向上への指針を示すことを目標とする．

2　遺伝子導入実験

2-1.　実験系

Fig.1 に実験装置の概略図を示す．ファンクションジェネレータ(NF 社製 WF1944A)からのバースト波をアンプ(E&I 社製 2100L)により，出力を増幅させて，トランデューサから平面波として，超音波を発生させた．周波数は 2.00 MHz とし，Duty Cycle 10 %(40/360)のバースト波として照射した．細胞を 24 well プレート内で培養し，マイクロバブルと導入する遺伝子を混合した培養溶液にトランスデューサを浸し，上部から超音波を照射した．遺伝子を導入させる細胞はマウス線維芽細胞系(NIH3T3)を用いた．線維芽細胞は多機能な未分化細胞で，軟骨への分化誘導遺伝子を細胞外から導入することで軟骨組織の再生治療へ応用が期待されている．導入する遺伝子は，レポーター遺伝子である GFP plasmid を用いた．細胞内に導入されると蛍光タンパク質が生成され，遺伝子が導入された細胞の特定が可能となる．また，マイクロバブルは超音波造影剤として用いられている Sonazoid®を用いた．

2-2　遺伝子導入実験

遺伝子導入率は超音波照射 48 時間後にフローサイトメトリーにより測定した．これは，GFP plasmid が細胞内に導入されると 48 時間後をピークに細胞内に蛍光が見られるためである．超音波を照射していない細胞をコントロールとして蛍光強度の閾値を定めることで遺伝子導入細胞を定義し，全生存細胞数に対する遺伝子導入細胞の割合として遺伝子導入率を求めた．実験条件は，GFP plasmid 濃度を 15 μg/ml，マイクロバブル数密度を 1.7×10^5 count/mm^3 と設定し，超音波強度と超音波照射時間をパラメータとした．実験結果を Fig.2，Fig.3 に示す．超音波強度が高いほどまた，超音波照射時間が長いほど，遺伝子導入率も向上しているといえる．ただし，本研究の実験条件下においては遺伝子導入率が 1 %以下と大変低くなっている．

2-3.　遺伝子導入現象の分析的検討

超音波強度をさらに大きく，かつ照射時間をさらに長くするほど遺伝子導入率の向上が期待される．しかしまず，行った実験条件下において遺伝子導入率が低い原因を特定し，遺伝子導入現象を以下のように要素的現象に分解し，それぞれについて検討することで，更なる遺伝子導入率向上を目指す．

①超音波照射により細胞膜に小孔が生じる．
②生じた小孔を通じて細胞内に遺伝子が取り込まれる．
③超音波及びマイクロバブルの作用を受けた細胞が生存する．
④細胞内で遺伝子が発現する．

本研究では，まず，評価可能な①及び③について検討する．

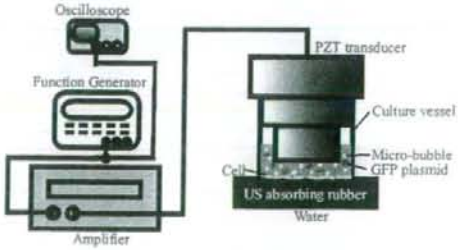

Fig.1　Experimental apparatus

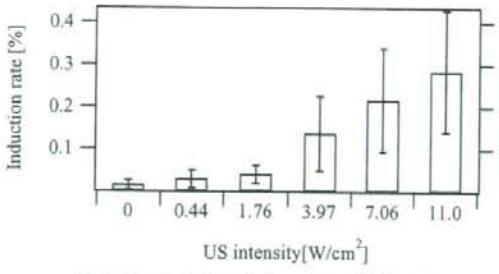

Fig.2 Gene induction rate dependent on US intensity
(US exposure time 60 s)

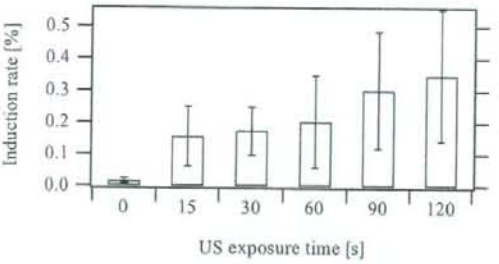

Fig.3 Gene induction rate dependent on US exposure time
(US intensity 1.76 W/cm^2)

3. 細胞生存率測定

超音波照射により細胞内に高い確率で遺伝子が導入されたとしてもその導入された細胞が生存する確率が低いとすると最終的な遺伝子導入率は小さくなる．そこで，細胞の生存について論じるために，超音波照射後の細胞生存率を細胞毒性試験試薬 Cell Counting Kit 8 (以下 CCK8)を用いて測定する．CCK8 は生細胞の代謝により還元され，橙色の formazan が生成される．formazan 生成量は生細胞数に比例するため，コントロールの吸光度に対するサンプルの吸光度を求めることで生存率を求められる．超音波照射直後，及び 48 時間後に細胞に CCK8 を加え，3 時間程度呈色反応させた後に吸光度を測定した．結果を Fig.4, Fig.5 に示す．この結果から，照射直後，48 時間後ともに 80 %程度の細胞が生存していることが明らかとなった．そのため，遺伝子導入率向上のためには残った生存細胞について分析する必要がある．

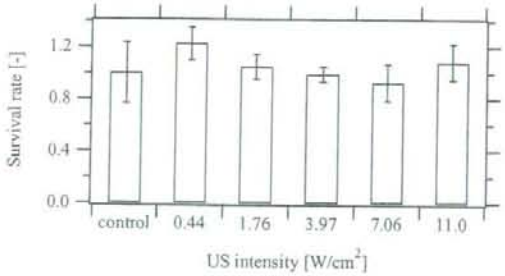

Fig.4 Cell survival rate (shortly after US exposure)

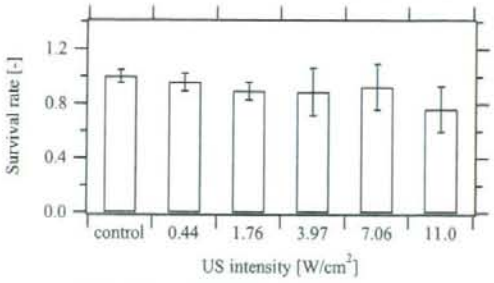

Fig.5 Cell survival rate (48 hours after US exposure)

4. 小孔形成細胞の可視化

ここでは細胞に小孔が生じていることを確認する実験について述べる．細胞に小孔が形成されたことは Propidium Iodide(以下 PI)を用いて確認できる．PI は細胞の核を染色する作用があるが，生細胞の膜を透過できないため，小孔が生じた細胞の核のみが染色される．超音波照射時に PI を培養液中に混和することで小孔形成細胞の特定が可能となる．本実験では蛍光観察により可視化を行った．超音波強度を 1.76 W/cm^2，照射時間を 60 s とした．Fig.6 に明視野観察画像を，Fig.7 に同位置での蛍光観察画像を示す．これらより大多数の細胞に小孔が生じていることが判明した．

Fig.6 Bright field image

Fig.7 Fluorescence image

5. 結言

超音波照射条件を変化させて遺伝子導入率を測定することにより，超音波強度を大きくするほど照射時間を長くするほど遺伝子導入率が向上することを確認した．しかし，実験条件下においては 1 %以下であった．生存率測定と小孔形成細胞の可視化を行った結果，80 %程度の細胞が生存しており，また多くの細胞に小孔が形成されていることが判明した．したがって，遺伝子が細胞に取り込まれない，または遺伝子が発現しないことが，遺伝子導入率が低い主因であると示唆される．このことを明らかにすることが今後の課題である．

謝辞

本研究の一部は，文部科学省「ナノバイオインテグレーション(CNBI)」，ならびに科学研究費補助基盤研究(A)1820620 による支援を受けました．ここに謝意を表します．

参考文献

[1]Taniyama et. al, "Local Delivery of Plasmid DNA Into Rat Carotid Artery Using Ultrasound", Circulation. 2002, pp.1233-1239.

Proceedings of Symposium on Ultrasonic Electronics, Vol. 29 (2008) pp. 291-292
11-13 November, 2008

Study of effect in active path selection of fluid microcapsules to the variation of ultrasound emission at the bifurcation point

流路分岐部における照射超音波の変化に対するマイクロカプセルの流路選択効率の検討

Yusuke Muramatsu[1‡], Sawami Ueda[1], Ryusuke Nakamoto[1], Yusuke Nakayashiki[1], Kohji Masuda[1], and Ken Ishihara[2] ([1] Tokyo Univ. Agri.& Tech.; [2]Ehime Univ.)
村松悠佑[1‡], 上田沢美[1], 中元隆介[1], 中屋敷悠介[1], 桝田晃司[1], 石原謙[2] ([1]東京農工大; [2]愛媛大)

1. Introduction

Making use of the phenomena that microcapsules or microbubble of μm order collapse themselves after ultrasound emission near their resonant frequency, physical DDS (Drug Delivery System) has been proposed[1,2]. To minimize the side effect of medication, drug should affect to the target area, not to other parts inside human body. Though recent mainstream of DDS is focused on the gene transduction by using gene vector, it takes time and cost to develop for each object. The microcapsules, which can contain the specified drug inside the shell, have the possibility to correspond to various kinds of medications. The distribution of the capsules is easily recognized by echogram (B-mode image) because the brightness of echogram varies according to the density of capsules. However, it was difficult to enhance the efficiency of medication because the capsules diffuse after the injection, where motion of the capsules in the blood flow cannot be controlled. In this paper we describe our attempt for active path selection of microcapsules in the artificial blood vessel by acoustic radiation force[3].

2. Experiment

We used microcapsule F-80E(Matsumoto Oil, Japan) which shell is made of PVC(polyvinyl chloride) with specific gravity as 0.0225 and average of diameter as 99.2 [μm]. We sieved it as the range of diameter is from 65 to 73 [μm] because of the limitation of magnification in the microscope. Also we have prepared the artificial blood vessel, which is made of PEG(polyethylene glycol), including the Y-form bifurcation as **Fig.1**. The external size is 50x80x10 [mm] and inner diameter of the path is 2 [mm]. The axis of the transducer is set 50 [deg] to *x-y* plane and 60 [deg] to *y-z* plane as shown in **Fig.2**. Defining the point O as the intersection of three paths, the points P, Q and R indicate 1, 2 and 3[mm] upper from O, respectively.

masuda_k@cc.tuat.ac.jp

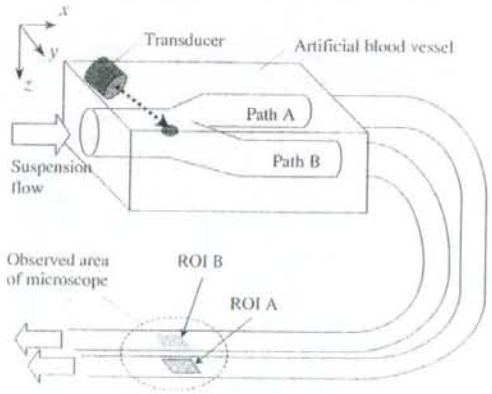

Fig.1 Experimental setup including artificial blood vessel.

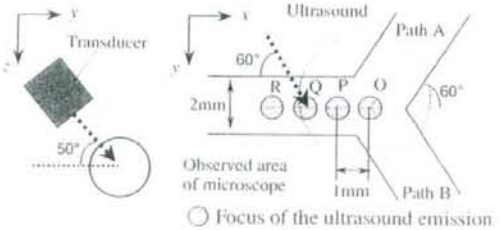

Fig.2 Schematic view of the artificial blood vessel

To evaluate the amount of capsules which passes through each path, we have extended two lower courses by using semi-transparent tube and established the observed area which includes them in the same view as shown in **Fig.1**. By using a microscope (BX50, Olympus, Japan), optical image of observed area is recorded.

3. Results

Fig.3 shows microscopic images of the area, which are captured by using high-speed camera Phantom-V4.2 (Nobby tech Co. Ltd, Japan) with interval time as 2 [ms]. To measure the capsules

amount, we established two square regions of interest in each course (ROI A, ROI B) and calculated the brightness average. The brightness in a region decreases according to the number of capsules inside. Thus we defined the shadow index as the following equation to evaluate the amount of capsules in the ROI.

$$\text{shadow index} = REF - \frac{\sum_{x=0}^{m}\sum_{y=0}^{n} f(x,y)}{S} \quad (1)$$

Where f is brightness of the ROI, REF is brightness average without capsules and S is area of the ROI. Then we have confirmed the relation between shadow index and capsules density.

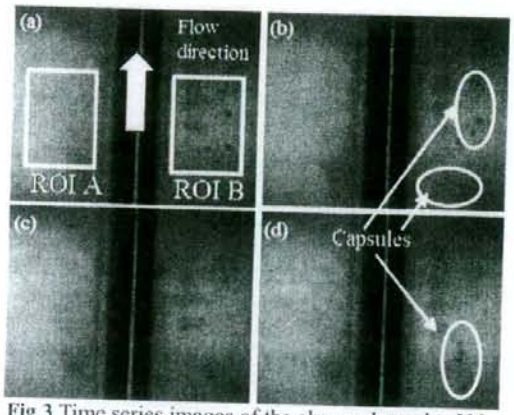

Fig.3 Time series images of the observed area by 500 [fps] after injection of capsules suspension with ultrasound emission.

Capsules suspension passed through the ROI without ultrasound and calculated the average of shadow index for 15 [frames] (duration 30 [ms]) for various flow velocities. As the result shown in **Fig.4**, using the density in capsules as 0.15-0.25 [g/L], significant change of density can be detected.

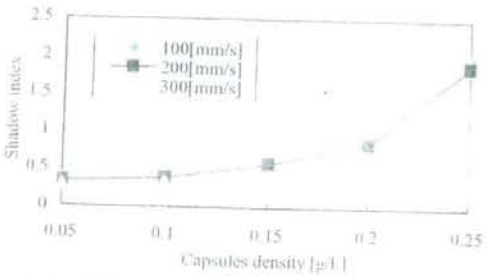

Fig.4 Shadow index versus capsules density.

We measured the shadow indices in two ROIs using various conditions in emission of sinusoidal ultrasound. When frequency as 1 [MHz], sound pressure as 160 [kPa], flow velocity as 100 [mm/s] and capsules density as 0.2 [g/L], ultrasound was focused at points O, P, Q shown in **Fig.2**. **Fig.5** shows the value of shadow indices for each focused point.

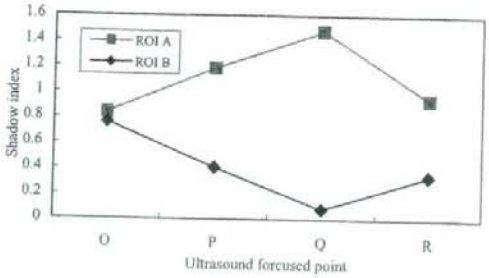

Fig.5 Capsules path selection efficiency depending on the ultrasound focused position.

When the ultrasound was focused at point O, there was no difference between two ROIs. However, more than 90 [%] of capsules were introduced to path B when the ultrasound was focused at point Q. Thus focused point of ultrasound emission and the shape of the bifurcation should be considered to realize active path selection of capsules.

4.Discussion

In this study, we used the microcapsules which size is 63~75[μ m] which cannot be applied to *in vivo* experiment. Because acoustic radiation force is proportional to the volume of capsules, it should be 1/100 when the diameter of capsules is several microns. Thus the blood velocity to be applied this technique is limited to few [mm/s]. Therefore we have to devise the minimization of the artificial blood vessel and its observation system.

5.Conclusions

In this study, we have experimented and considered to realize active path selection of microcapsules at a bifurcation of the artificial blood vessel. We are going to apply the experiment by varying other parameters and to investigate the mechanism of this phenomena.

References

1. D. Koyama, W. Kiyan and Y. Watanabe : Jpn. J. Appl. Phys. 43 (2004) 3215-3219.
2. Y. Yamakoshi and M. Koganezawa : Jpn. J. Appl. Phys. 44 (2005) 4583-4587
3. Y. Muramatsu, K. Masuda, S. Ueda, K. Ishihara : Proc. Symp. Ultrason. Electron, Vol.28, (2007), 407-408.

生体医工学
46(2): 275-282, 2008

超音波定在波の印加による流路中のマイクロカプセルの局所的濃度制御とその観測

桝田 晃司*・村松 悠佑*・溝部 一行*・石原 謙**

Control Method of Local Density in Fluid Microcapsules by Acoustic Standing Wave and its Monitoring

Kohji MASUDA,* Yusuke MURAMATSU,* Ikkou MIZOBE,* Ken ISHIHARA**

Abstract We have developed control method of local density in fluid microcapsules to make use of ultrasound drug delivery system. It has been difficult to enhance the efficiency of medication because capsules solution diffuses after the injection, where motion of capsules in blood flow cannot be controlled. Then we have noticed that microcapsules are trapped by acoustic standing wave of ultrasound in water. We have applied this method to an artificial blood vessel and observed the variation of capsules density by using the software, which we have developed to detect local change of the brightness variation on echogram. The result indicated that capsules density increases in the upper course of the point where the standing wave is produced. We have also prepared another artificial blood vessel with bifurcation in it. We have recorded echogram of two lower courses after the bifurcation and evaluated the brightness average of the two regions in each course, when the standing wave is produced at a lower course near the bifurcation point. As the result, we confirmed that the density in microcapsules decreases when standing wave is put on the course, where the density increases on the other course. It shows a possibility to control microcapsules direction and to lead to an objective point in blood vessel.

Keywords: ultrasound DDS, microcapsule, acoustic standing wave, echogram, artificial blood vessel.

1. はじめに

薬物治療は医療の黎明期より存在し，経口・塗布・注射といった投与法があるが，体内に投与された薬物は目的部位まで運ばれる過程で拡散し，また肝臓・腎臓で捕捉・排泄されるため，目的部位での十分な薬物効果を得るためには投与時に高い薬物濃度が必要である．一方，投薬量を増やすと他の部位での副作用が発生するという問題がある．このため，患部にのみ必要量の薬物を送り，最大限有効な薬物効果を得る選択的薬物伝送システム（Drug Delivery System．以下 DDS）が数多く研究されている．現在，主流は遺伝子操作等のバイオテクノロジーを用いた化学的手法で，薬物に修飾基を合成することで，標的指向性や吸収性を付加する等の手法があるが，薬物ごとに異なる修飾基を用いる必要があるため，開発に時間がかかりコストが高くなる等の問題点が存在する[1]．

一方，物理的手法による DDS として，直径数～数十ミクロンのマイクロカプセルを超音波により生体内で破壊する手法[2-4]が提案されてきた．これらは音波による物理的作用を利用するもので，まず薬物を含んだマイクロカプセルを生体内に注入し，生体外からある条件の超音波を照射することにより，マイクロカプセルのシェルを膨張・収縮させ破壊する．マイクロカプセルはそれ自身が超音波造影剤となるため，目的部位への到達確認と破壊のモニタリングを超音波のみで行うことができる[3]．カプセル内に薬物を保持させる手法としては，薬物が気化した状態でカプセルを製造するか，カプセルの殻自身に薬物を含ませる手法等[5]が考案されている．

これまでに行われた超音波 DDS を目指した研究として，高速度カメラを用いた超音波音場での気泡の観察[6, 7]，B モード像の深さ方向に対する輝度変化からのカプセル濃度の推定[8]，定在波によるマイクロバブルの捕捉[9]と破壊[10]，また衝撃波を用いる手法[11]や，破壊による細胞膜への損傷効果[12, 13]等の研究が行われてきた．また粒

生体医工学シンポジウム 2007 発表．2007 年 9 月，札幌
2007 年 8 月 2 日受付，2007 年 11 月 7 日改訂，2007 年 12 月 4 日再改訂
Received August 2, 2008; revised November 7, 2007, December 4, 2007.
* 東京農工大学大学院 生物システム応用科学府
Graduate School of BASE, Tokyo Univ. A&T
** 愛媛大学医学部附属病院 医療情報部
Dept. of Medical Informatics, Ehime Univ. Hospital

径の異なる複数の気泡を凝集させる研究[14]も行われているが，生体内へ注入後のカプセルは血流の抵抗を受けることを考慮しなければならず，その挙動や動態を生体外から能動的に操作し，モニタリングする手法は確立されていなかった．

ところで音波によって作用する音響力を利用する技術として，物体を非接触で空間中に保持できる音波浮揚あるいは超音波マニュピレーション[15, 16]が知られている．超音波の定在波によって形成される節または腹において，血球レベルのマイクロカプセルを捕捉できることは，これまでに光学的観察[17, 18]によって明らかにされている．

そこで本研究は，体外からの超音波照射により，生体内のマイクロカプセルに音響力を作用させ，その濃度や動態を局所的に制御すると同時に，超音波断層像によってリアルタイムの *in vivo* 観察・計測を行うシステムを構築することを目的とする．超音波によって局所的なカプセル濃度を自在に制御できるDDSが実現すれば，投薬量の調節が可能となり，カプセル破壊のためのエネルギーを抑えて生体に対するリスクを低減することができる．また血管の分岐部において局所的濃度変化を与えることができれば，カプセルの流路を選択して目的部位への誘導が可能となる．つまりカプセル放出から標的部位までに多数の経路が存在していたとしても，その中から最適な流路を設定し，カプセルを誘導できるようになると考えられる．

2. 方　　法

2・1　マイクロカプセルとその懸濁液の作成

本研究ではマイクロカプセルとして，熱可塑性高分子（AN系コポリマー）の殻を有し，炭化水素（イソブタン）を内包した松本油脂社製マイクロスフェアーを用いる．これは本来，立体プリント用断熱材や緩衝剤等として使われているもので，生体適合性には問題があるが，本実験で用いる範囲の音圧の変化や流速に対して安定である．図1はF-80E（真比重0.0225，平均粒径99.2 μm）をふるいにかけ，粒径63~75 μm に選別したカプセルの顕微鏡画像である．

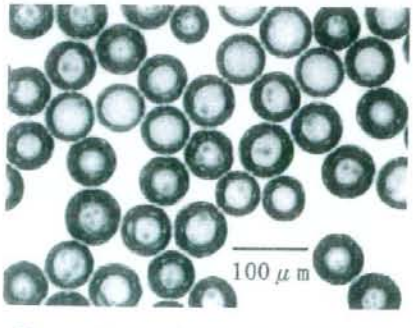

図1　マイクロカプセルF-80Eの顕微鏡写真
Fig. 1　A photomicrograph image of microcapsule F-80E.

以下，カプセル懸濁液の作成法を述べる．マイクロスフェアーF-80Eは粉体の状態で存在するため，サンプルから重量 W g のカプセルを抽出する．顕微鏡で確認したところ，粒径30 μm 以下のものから120 μm 程度のものまで含まれている．そこでカプセルを水に溶かして懸濁液を作成し，開口幅（目開き）38，63，75，90 μm のマイクロシーブ（ふるい）を用いて粒径を選別する．一旦懸濁液の状態にするとカプセルそのものの重量は計測できないので，予め顕微鏡画像上で計測していた各粒径範囲に対する存在確率 α から，粒径を選別された懸濁液中のカプセルの重量 αW g を算出する．その値を懸濁液の体積 L l で除算し，次式のように懸濁液の濃度（重量濃度）d g/l を得る．

$$d = \alpha W / L \qquad (1)$$

2・2　模擬血管とBモード像による観測

本研究では，マイクロカプセルの局所的な濃度変化の *in vivo* での観測手段として超音波断層像（以下，Bモード像）を採用する．一般にBモード像上の輝度は，超音波反射体と周辺組織の音響特性の相対関係によって変化するが，カプセル内の気体の音響インピーダンスは生体組織と大きく異なるため，反射率はほぼ100%であると考えられる．よって生体内のカプセルにて反射したエコー信号は，カプセルの濃度と相関があると予想される．通常，輝度値はプローブからの距離や診断装置のゲイン調整等で簡単に変動する性質があるが，診断装置の設定を固定し，濃度変化に対する輝度変化が線形になる条件において，濃度変化の測定は可能[19]である．

模擬血管として，超音波透過性に優れたポリエチレングリコールを外径40 mm，内径12 mm，長さ100 mm の中空円筒の形状に成形した．外径が内径の6倍以上であるのは形状の安定性を保つためで，また内径のサイズは，後述するBモード像上での輝度平均を計算する領域を確保する必要があるためである．この模擬血管を図2に示すように水で満たされた水槽中に沈め，ロータリーポンプ，流量計を含む流路システムに組み込んでマイクロカプセル懸濁液を流す．懸濁液は注射器等で注入すると拡散し，濃度が大きく低下するため，図中に示すように三方コックを用いて

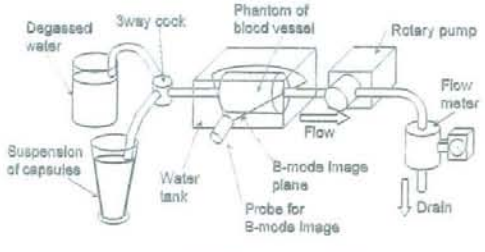

図2　カプセル懸濁流観測のための流路システム
Fig. 2　Flow system to observe suspension of capsules.

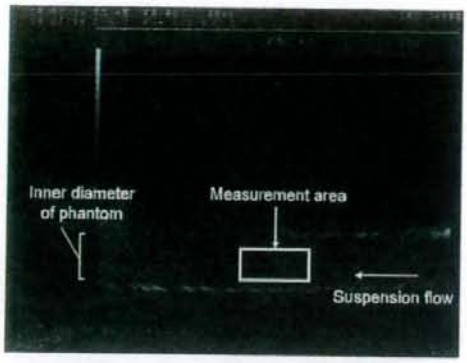

図3　模擬血管の断面と懸濁液の流れ
Fig. 3　B-mode image of the phantom and suspension flow.

予め脱気水を流しておき，コックを切り替え，模擬血管内にカプセル懸濁液が流入した状態のBモード像を記録する．輝度変化の計測は，カプセル懸濁液が通過し始めた後から定常状態に達した以降とする．

超音波診断装置は日立メディコ社製EUB-565S，中心周波数3.5 MHzのセクタ走査型プローブを使用する．セクタ走査を選択したのは，模擬血管の長さ方向全体に渡って観察するためで，プローブ表面からの深さ70 mm程度において模擬血管全体を観察できるように設定した．得られるBモード像を図3に示す．

Bモード像のPCへの取り込みは，画像入力ボード(FLX-PCI，フォトロン)を介してフレームレートを30 fpsでハードディスクに記録する．またBモード像上の任意に設定した領域の輝度平均値を算出するために，VisualC++とDirectX9.0を用いて開発したプログラム[20, 21]を適用する．領域の形状，サイズ及び位置は画面上に配置したボタンで，それぞれ1 pixel単位で自由に設定可能である．また領域の輝度平均値の時系列変化をMicrosoft Excelにて表示・保存することができる．領域内の輝度平均値は，各フレーム内での領域内の輝度の平均値を，計測に要した全てのフレームにおいて平均するものとする．

2·3　流路を横断する定在波の形成

上記の実験系で，模擬血管中のカプセル懸濁液の流れを横断する方向に，中心周波数1 MHzの収束型狭帯域超音波トランスデューサ（NTR Co. Ltd., PA072）を設置し，正弦波を高周波増幅器（サムウェイA50-1601）にて増幅することにより，水槽底面との間で定在波を形成する．トランスデューサの中心周波数は，カプセルの共振周波数[22]である数十～百数十kHzの周波数から外れており，また波長が1.5 mmであることから，模擬血管内に定在波の節と腹が数個ずつ存在することになる．トランスデューサは直径25 mmの円筒形で，照射面から中心軸上45 mmのところで放射音圧が最大（半値幅約3 mm）になることから，水槽底面との距離を45 mmに保つことによって水槽底面からの反射強度を確保する．定在波音場の音圧の計測は困難であるが，水槽底面における反射音圧の最大値を定在波の音圧とする．また，この実験系を用いて静水中に定在波を形成し，上記のマイクロカプセルを捕捉できることは既に確認している[23]．

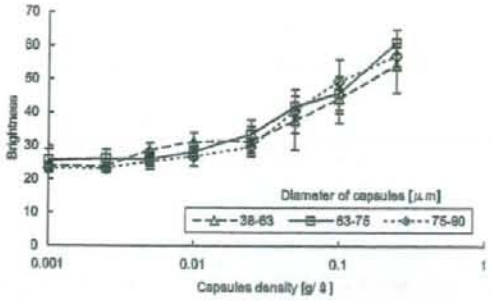

図4　カプセル濃度に対する模擬血管中の設定領域の輝度値
Fig. 4　Brightness average in the specified region of B-mode of the phantom versus capsules density.

実際に人体に適用する場合は，生体内に反射板等を設置するのは困難であり，複数の音源からの音波の干渉によって定在波を形成する手法[14]は既に研究されているが，本論文では模擬血管の形状の都合上，1個のトランスデューサによって定在波を形成した．

3．結　　果

3·1　カプセル濃度に対するBモード像上の輝度変化

カプセル濃度に対するBモード像上の輝度の変化を確認するため，粒径によって選別した38～63，63～75，75～98 μmのそれぞれのカプセル懸濁液を0.001～0.2 g/ℓの濃度範囲で作成し，流速を100 mm/sとして図2の模擬血管に流した．カプセルの反射率が高いことから，診断装置の輝度のゲイン（明るさ調整）は最小値の－30 dBとして固定した．輝度の測定領域は図3に示した箇所，プローブ表面から深さ60 mmの16×8 mmの領域とした．図2中の三方コックを切り替えた後，カプセル懸濁液は模擬血管を通過するが，脱気水との境界では泡が含まれる場合があるため，切り替え後定常状態に達する2～3秒後から約5秒間程度を計測時間とした．この実験を同一の濃度に対して3回繰り返して計測した．

各濃度に対するBモード像上での測定領域の輝度平均値の関係を図4に示す．各粒径とも，濃度の上昇と共に輝度が上昇する傾向を示した．粒径による違いは大きく見られなかったが，0.01 g/ℓ以上の濃度では輝度値から濃度を推定可能なことが分かった．ここで0.2 g/ℓより高い濃度で実験をしなかったのは，不均一な固まりが生じて懸濁液とならなかったためである．この結果より輝度変化を顕著に示す濃度が0.1 g/ℓ付近であることから，以下の実験ではこの濃度を使用することとする．

3・2　定在波の印加による局所的カプセル濃度の変化

図2の実験系に，定在波を印加するトランスデューサを追加した．模擬血管に対する配置を**図5**に示す．x軸方向に走る模擬血管に対し，z軸方向から定在波を印加し，管内にカプセル溶液を注入する様子をy軸上に置いた超音波プローブでxy平面のBモード像を観察した．この時得られるBモード像を**図6**に示す．定在波が印加される位置は図中の中央，丸印に相当する．さらにその左右に計4つの計測領域を設定し，定在波印加位置を中心にして上流方向にR1，R2，下流方向にL1，L2とした．各領域は長方形でサイズは6×9 mm，L1とR1の間隔を定在波のビーム径（半値幅）よりも大きい5 mmとした．

カプセル粒径を38～63，63～75，75～98 μmに選別し，濃度を0.1 g/lとしたそれぞれの懸濁液を流速100 mm/sで模擬血管内に流した．定在波の周波数は1 MHz，水槽底部における定在波の最大音圧は150 kPaとした．定在波の有無それぞれの場合において，懸濁液の流入後，定常状態に達してから5秒間Bモード像を記録し，各領域の輝度平均値を計測した結果を**図7**に示す．定在波を印加していない状態でL2とR2の輝度が高いのは，セクタ走査のために端点に近づくほど空間分解能が低下することが影響している．定在波が印加された状態では，印加位置を境にカプセルの輝度に変化が生じ，上流領域ではカプセル濃度は上昇し，下流領域では下降する傾向が見られた．またカプセルの粒径が大きいほど，上流と下流の輝度差が大きくなった．ここで下流領域での輝度値が減少したのは，カプセル自身が破壊した可能性も考えられたが，前述したように定在波の周波数はカプセルの共振周波数より一桁小さく，ま

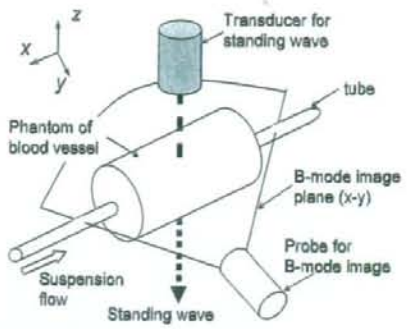

図5　模擬血管中への定在波の形成とBモード像による観察
Fig. 5　Production of standing wave in the phantom and observation by B-mode image.

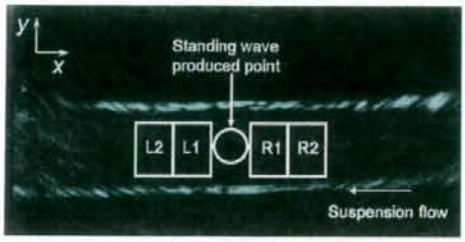

図6　定在波照射位置に対する模擬血管中の輝度測定領域の設定
Fig. 6　Establishment of 4 measurement regions of the phantom by centering the point of standing wave.

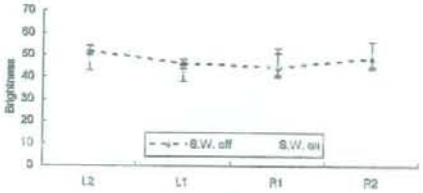

(a) D= 38-63[μm]

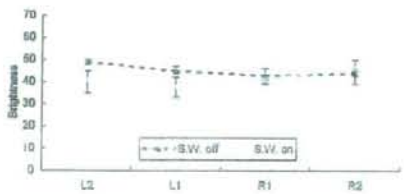

(b) D=63-75[μm]

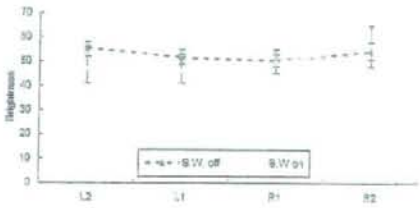

(c) D= 75-90[μm]

図7　各カプセル粒径における定在波の有無と各設定領域の輝度平均値の比較
Fig. 7　Comparison of brightness in the measurement regions versus existence of the standing wave on several capsule diameters.